Phosphorescence Spectra and Excited States Dynamics of Chlorotoluenes in a Rigid Glass Matrix

Tetsuo Okutsu,* Naomi Kounose,† Jun Tsuchiya, Tadashi Suzuki,†† Teijiro Ichimura,†† and Hiroshi Hiratsuka

Department of Chemistry, Gunma University, Kiryu, Gunma 376-8515

†School of Health Sciences, Gunma University, Maebashi, Gunma 371-8514

††Department of Chemistry, Tokyo Institute of Technology, Ohokayama, Meguroku, Tokyo 152-8551

(Received December 10, 1999)

The excited-state dynamics of chlorobenzene (CB), *o*-chlorotoluene (*o*-CT), *m*-chlorotoluene (*m*-CT) and *p*-chlorotoluene (*p*-CT) have been investigated in 3-methylpentane at 77 K. The phosphorescence spectra of CB and *o*-CT show a maximum at around 510 nm, while the maxima of *m*-CT and *p*-CT are 450 and 420 nm, respectively. These phosphorescence spectra are divided into dual phosphorescence spectra: namely $^3\pi\pi^*$ and $^3\pi\sigma^*$ phosphorescence. The large phosphorescence peak-shifts among the chlorotoluenes are ascribable to a lowering of the low-lying $^3\pi\pi^*$ state. The intersystem-crossing (ISC) quantum yields from S_1 to $^3\pi\pi^*$ ($\phi_{ISC}^{\pi\pi^*}$) depend on the samples, whereas $\phi_{ISC}^{\pi\sigma^*}$ from S_1 to $^3\pi\sigma^*$ are independent of the sample. These results have been explained in terms of the vibrational Franck–Condon overlap between the S_1 state and triplet manifolds.

The photoreaction of halogenated benzenes in the triplet state have received attention, and it has been revealed that the triplet state predominantly photodissociates to the phenyl radical and halogen atom.[1—10] In a rigid glass solution the phosphorescence spectra of halogenated benzenes were reported to be dual phosphorescence originating from two low-lying triplet states, $^3\pi\pi^*$ and $^3\pi\sigma^*$.[11—16] Takemura et al. investigated the kinetic behavior of the phosphorescent triplet states of chlorobenzene (CB), *p*-dichlorobenzene and *p*-dibromobenzene.[11] Dual phosphorescence is composed of a slow-decaying component due to the transition $^3\pi\pi^* \rightarrow S_0$ and the fast decaying component due to the transition $^3\pi\sigma^* \rightarrow S_0$.[17,18] The apparent activation energies have been determined for a mutual conversion process between the two triplet states.

Nagaoka et al. have reported on the potential-energy surfaces of low-lying triplet states of CB using the ab-initio unrestricted Hartree–Hock (UHF) method.[18] They reported that the C–Cl equilibrium bond length in the $^3\pi\pi^*$ state is close to that of the ground state, while $^3\pi\sigma^*$ states are bonding at much longer C–Cl bond distances, with the lengthening amounting to about 0.6 Å.

In our previous study, it was reported that *p*-CT emits dual phosphorescence and that the rate of the intersystem crossing from S_1 to $^3\pi\pi^*$ and $^3\pi\sigma^*$ depended on the temperature and solvent, and also that the non-radiative decay rate constants strongly depended on the viscosity of the solvent.[19] Utilizing this solvent effect on the enhancement of the phosphorescence quantum yield, we could successfully observe the phosphorescence spectrum of bromobenzene in a highly glassy matrix.[20]

The main difference in the spectrum of *p*-CT compared with that of CB is a large peak-shift to shorter wavelength: those peaks are 420 and 510 nm at 77 K for *p*–CT and CB, respectively. The other chlorotoluens, *o*-CT and *m*-CT, show different peak positions from either CB or *p*-CT. In the present study, we investigated the kinetic properties of the low-lying excited states of the *o*-, *m*- and *p*-CT, and experimental results were compared with the results obtained by MO calculations.

Experimental

Chlorobenzene (Kanto Chemical, G.R.), *o*-chlorotoluene (Tokyo Chemical, G.R.), m-chlorotoluene (Tokyo Chemical, G.R.) and *p*-chlorotoluene (Wako Chemical, G.R.) were purified by vacuum distillation. 3-Methylpentane (Tokyo Chemical, spectral grade) was purified by distillation.

The experimental setups were described in a previous paper.[20] Absorption spectra were measured by using a Hitachi U3300 spectrophotometer. Emission spectra were measured by a Hitachi M-850 spectrophotometer. Time-resolved phosphorescence spectra and lifetimes were simultaneously obtained using a UNISOKU TSP-601H nanosecond laser flash photolysis system with a Nd^{3+}: YAG laser (266 nm output of fourth harmonic, pulse width 10 ns, GCR-130, Spectra Physics) and an oscilloscope (GOULD 4090).

Result and Discussion

Figure 1 shows the phosphorescence spectra of chlorobenzene (CB), *p*-CT, *o*-CT, and *m*-CT in 3MP at 77 K. Since the excitation spectra of *o*-CT and *m*-CT are similar to each absorption spectrum, the observed emissions are assigned

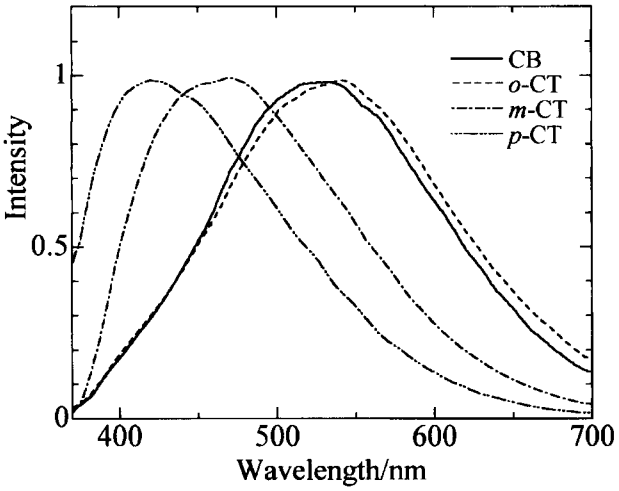

Fig. 1. Steady-state phosphorescence spectra of CB (—), *o*-CT (- - -), *m*-CT (– · –), and *p*-CT (– · · –), excited at 266 nm in 3-methylpentane at 77 K.

to the phosphorescence of *o*-CT and *m*-CT. All emissions are broad and show no prominent vibrational structure. The phosphorescence quantum yields were determined to be 0.04, 0.14, and 0.19 for *o*-CT, *m*-CT, and *p*-CT, respectively, by comparing with the reported value of toluene, $\phi_p = 0.26$.[21] The phosphorescence peaks were observed at 420, 450, 510, and 500 nm for *p*-CT, *m*-CT, *o*-CT, and CB, respectively. It is interesting that the difference in methyl substitution position brings about such large phosphorescence shifts. The phosphorescences of CB and *p*-CT are reported to exhibit dual phosphorescence, which are composed of shorter-wavelength emission with a longer lifetime from the $^3\pi\pi^*$ state and a longer-wavelength one with a shorter lifetime from the $^3\pi\sigma^*$ state.[11,20] The variety of the phosphorescence contours of chlorotoluenes suggests that the relative intensity changes between $^3\pi\pi^*$ and $^3\pi\sigma^*$ phosphorescence.

To obtain detailed information on the phosphorescence nature of chlorotoluenes, time-resolved measurements were carried out. Decay time-profiles of all samples could not be fitted by a single exponential decay function, but were successfully fitted by a bi-exponential decay function. At the temperatures concerned in this study, the phosphorescence decays monitored in the range of 350—700 nm were analyzed by bi-exponential function. The decay time profile of the phosphorescence intensity ($I_{p\lambda}(t)$) monitored at wavelength λ can be expressed in the form[22,23]

$$I_{p\lambda}(t) = C_s(\lambda)e^{-k_s t} + C_f(\lambda)e^{-k_f t}, \quad (1)$$

where k_s and k_f are the decay rate constants with $k_s < k_f$, i.e., s and f refer to the slow and fast decay of the phosphorescence, respectively. C_s and C_f are pre-exponential factors of the slow and fast components. The decay rate constants, k_s and k_f, have been confirmed to be independent of the monitoring wavelength, λ. Figure 2 shows plots of C_s/k_s and C_f/k_f against λ, which represent the resolved phosphorescence spectra of the fast and slow components for CB, *o*-CT, *m*-CT, and *p*-CT, respectively. The sum of C_s/k_s and C_f/k_f is similar

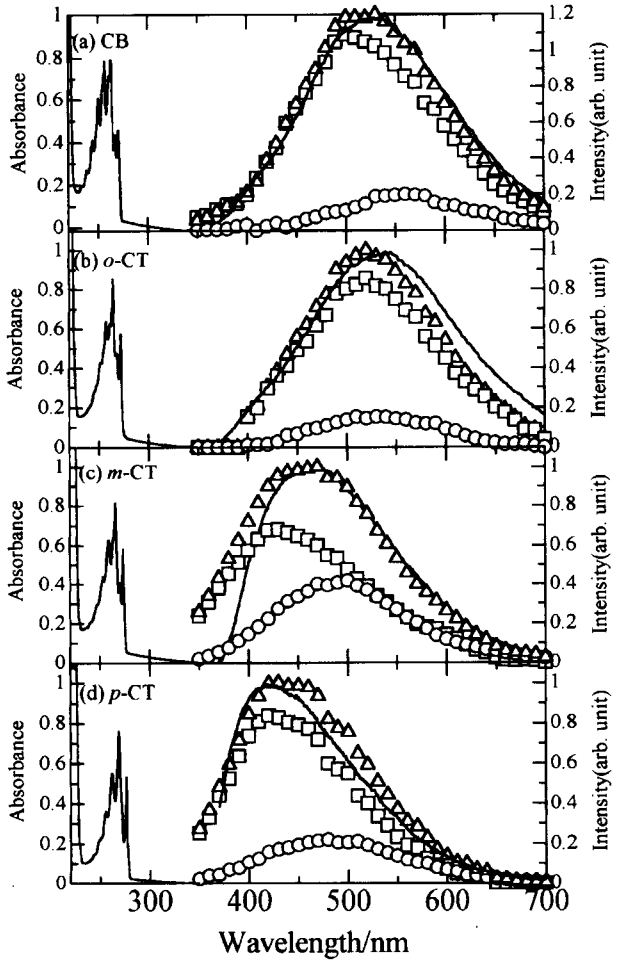

Fig. 2. Plots of C_s/k_s (□), C_f/k_f (○), sum of C_s/k_s and C_f/k_f (△) and steady-state phosphorescence, and absorption spectra of (a) CB, (b) *o*-CT, (c) *m*-CT and (d) *p*-CT.

to the steady-state phosphorescence spectra. Shorter lifetime phosphorescences are assigned to originate from $^3\pi\sigma^*$ and longer lifetimes ones are from $^3\pi\pi^*$ to the ground state, followed by the assignments of the dual phosphorescence of CB and *p*-CT. The quantum yields of the phosphorescences are determined by comparing each phosphorescence area with the total phosphorescence quantum yield; the results are listed in Table 1. The phosphorescence from the $^3\pi\sigma^*$ state shows a peak at around 500 nm independent of the sample, whereas the phosphorescence from the $^3\pi\pi^*$ state shows a peak at various wavelengths: peaks are at 500, 490, 430, and 420 nm for CB, *o*-CT, *m*-CT, and *p*-CT, respectively. The phosphorescence from the $^3\pi\pi^*$ state is found to be dominant for all samples. Thus, the reason for the different contours of the phosphorescence band is concluded to be due to the variation of the contours of the $^3\pi\pi^*$ phosphorescence, not the contribution change in the intensity between the dual phosphorescence. This is explained by the actual energy change in the triplet $^3\pi\pi^*$ states, themselves. The energy of the triplet state is known to differ from the same electronic singlet state by twice the exchange integral, $2J$. The absorption spectrum of the corresponding singlet state,

Table 1. Kinetic Paramenters for Chlorobenzene, *o*-, *m*-, and *p*-Chlorotoluenes in 3MP at 77 K

	Φ_p^{total}	$\Phi_p^{\pi\pi^*}$	$\Phi_p^{\pi\sigma^*}$	k_{rs}/s^{-1}	k_{nrs}/s^{-1}	k_{rf}/s^{-1}	k_{nrf}/s^{-1}	$\Phi_{ISC}^{\pi\pi^*}$	$\Phi_{ISC}^{\pi\sigma^*}$	A/s^{-1}	ΔE/kJ mol^{-1}
CB	0.07	0.06	0.01	220	510	440	1900	0.19	0.04	3.1×10^{14}	18
o-CT	0.04	0.04	0.01	200	1250	320	6400	0.25	0.13	7.8×10^{9}	11
m-CT	0.14	0.09	0.05	30	100	380	360	0.41	0.10	4.0×10^{15}	20
p-CT	0.19	0.15	0.04	40	100	330	370	0.54	0.09	5.1×10^{15}	20

$^1\pi\pi^*(^1L_a)$ band, around 250 nm is also shown in Fig. 2. In order of CB, *o*-CT, *m*-CT, and *p*-CT, the origin of the ^1L_a band was shifted to red, whereas the phosphorescence from the $^3\pi\pi^*$ state was shifted in the opposite order. Figure 3 shows plots of the peak-shift of the $^3\pi\pi^*$ phosphorescence from the peak of CB against the shift of the origin of the $^1\pi\pi^*$ band from that of CB. Although the plots of the peak-shift of the phosphorescence should be carried out to the origin of the phosphorescence, an ambiguity of the origin makes it impossible to clarify the origins of the emissions.

The electrostatic exchange integral, J, is given by the equation[24]

$$J = \iint \pi^*(x_1)\pi(x_1)\frac{e^2}{r_{12}}\pi^*(x_2)\pi(x_2)dx_1dx_2. \quad (2)$$

This is proportional to the overlap integral, $\langle\pi^*(1)|\pi(1)\rangle$, which were calculated by the PM3 method using the ground-state wavefunctions. The calculated values are also plotted in Fig. 3. Large exchange integral leads to a higher singlet energy and a lower triplet energy. Since the exchange integral is found to show a good relation with both the absorption and phosphorescence shift, the difference in the magnitude of exchange integral, J, is responsible for energy shift of the $^3\pi\pi^*$ state.

The predominance from the $^3\pi\pi^*$ state phosphorescence over that from the $^3\pi\sigma^*$ state is discussed as follows. There are two presumptions to explain the above mention of phenomenon. One is phosphorescence quantum yields, $\phi_p^{\pi\pi^*}$, which is larger than $\phi_p^{\pi\sigma^*}$. $\phi_p^{\pi\pi^*}$ and $\phi_p^{\pi\sigma^*}$ were determined by the radiative and non-radiative rate constants. The other is the change in the quantum yields of ISC from S_1 to the $^3\pi\pi^*$ and $^3\pi\sigma^*$ states. The above values are estimated as in the following manner.

The decay constants k_i (i = s or f) are expressed in the form

$$k_i = k_i^0 + A_i e^{-\frac{\Delta E_i}{RT}}, \quad (3)$$

where k_i^0 is the temperature-independent decay constant, which is mainly regarded as the phosphorescence radiative rate constant, k_r. A_i is a frequency factor and ΔE_i is the activation energy. These may correspond to the frequencies and energies of the vibrational modes which promote non-radiative decay processes. The second term in Eq. 3 is supposed to mainly indicate the rate constant of non-radiative decay process.[8] The values of k_i^0, A_i, and ΔE_i were determined by a least-squares fitting of the experimental results obtained at several temperatures. The non-radiative decay rate constant, k_{nr}, is obtained as $k_i - k_i^0$ (i = s or f).

The quantum yields of ISC to $^3\pi\pi^*$ and $^3\pi\sigma^*$ states were estimated by the following equations:

$$\phi_p^{\pi\pi^*} = \Phi_p^{total} \times \frac{I_{EM}^{\pi\pi^*}}{I_{EM}^{\pi\pi^*} + I_{EM}^{\pi\sigma^*}}, \quad (4)$$

$$\phi_p^{\pi\sigma^*} = \Phi_p^{total} \times \frac{I_{EM}^{\pi\sigma^*}}{I_{EM}^{\pi\pi^*} + I_{EM}^{\pi\sigma^*}}, \quad (5)$$

$$\phi_{ISC}^{\pi\pi^*} = \phi_p^{\pi\pi^*} \times \frac{k_r^{\pi\pi^*} + k_{nr}^{\pi\pi^*}}{k_r^{\pi\pi^*}}, \quad (6)$$

$$\phi_{ISC}^{\pi\sigma^*} = \phi_p^{\pi\sigma^*} \times \frac{k_r^{\pi\sigma^*} + k_{nr}^{\pi\sigma^*}}{k_r^{\pi\sigma^*}}, \quad (7)$$

where $I_{EM}^{\pi\pi^*}$ and $I_{EM}^{\pi\sigma^*}$ are the phosphorescence intensity of the $^3\pi\pi^*$ and $^3\pi\sigma^*$ states, respectively. The results are listed in Table 1.

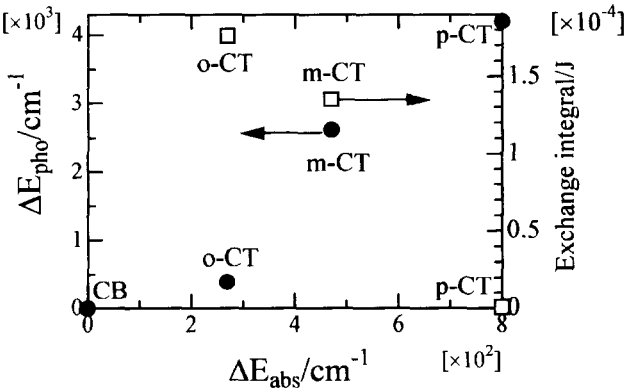

Fig. 3. Plots of the energy shift of the $^3\pi\pi^*$ phosphorescence (●) from that of CB and plots of the shift of the exchange integral (□) from *p*-CT against the energy shift of the $^3\pi\pi^*$ absorption from that of CB.

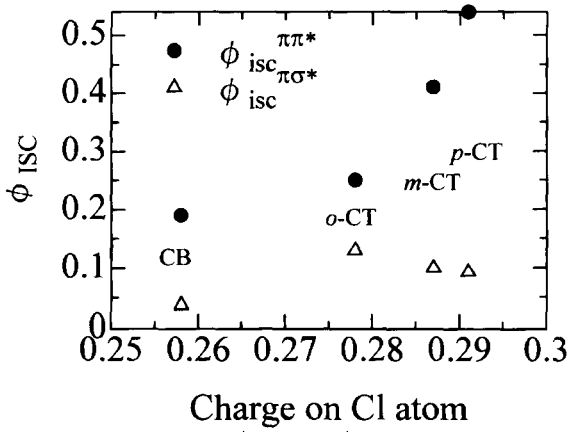

Fig. 4. Plots of the $\phi_{ISC}^{\pi\pi^*}$ and $\phi_{ISC}^{\pi\sigma^*}$ against the charge on the Cl atom at S_1 state.

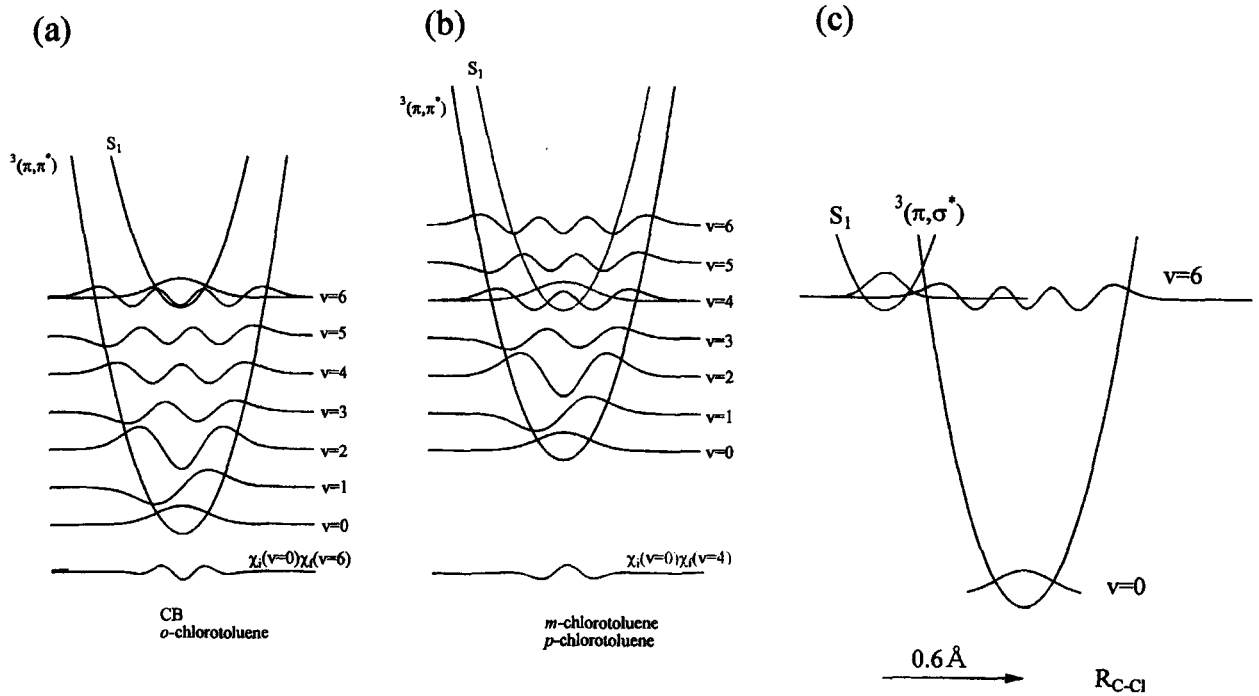

Fig. 5. Franck–Condon overlaps between S_1 state and $^3\pi\pi^*$ state of (a) for CB and *o*-CT and (b) for *m*-CT and *p*-CT, and Franck–Condon overlap between S_1 state and $^3\pi\sigma^*$ state.

The values of $\phi_{ISC}^{\pi\pi^*}$ are found to be larger than $\phi_{ISC}^{\pi\sigma^*}$ for all samples. The values of $\phi_{ISC}^{\pi\pi^*}$ depend on the samples, while those of $\phi_{ISC}^{\pi\sigma^*}$ are independent of the samples. Here, we discuss the difference of $\phi_{ISC}^{\pi\pi^*}$ and the similarity of $\phi_{ISC}^{\pi\sigma^*}$ among chlorotoluenes by making use of the results obtained by molecular-orbital calculations. The allowed ISC pathways from S_1 to triplet manifolds of CB are S_1 to the T_x sublevel of the $^3\pi\pi^*$ and S_1 to the T_z sublevel of the $^3\pi\sigma^*$ states. Though the molecular symmetries belong to C_{2v} only for CB, the same selection rules can be applied for ISC in the case of chlorotoluenes. The difference due to the substitution position is explained by the electron density on the Cl atom in the S_1 state, and by the Franck–Condon overlap between S_1 and the triplet manifold. The charges on the chlorine atom in the S_1 state, which are calculated by the MNDO-PM3 method, are plotted against $\phi_{ISC}^{\pi\pi^*}$ in Fig. 4. $\phi_{ISC}^{\pi\pi^*}$ are found to increase with increasing in electron densities on the chlorine atom. This effect is interpreted by the heavy atom effect due to the Cl atom. The Franck–Condon overlaps are discussed using the potential-energy function for the one-dimensional harmonic oscillator shown in Fig. 5. Here, a symmetric vibration mode of 3194 cm^{-1}, calculated by the MNDO-AM1 method, is chosen as an accepting mode of the triplet manifold. For CB and *o*-CT, the vibrational wave function, χ_i, of S_1 corresponds to the $v = 0$ level, and the vibrational wave function of the $^3\pi\pi^*$ state, χ_f, corresponds to the $v = 6$ level, which is derived from the energy difference between S_1 and the $^3\pi\pi^*$ state. For *m*-CT and *p*-CT, since the energy of the $^3\pi\pi^*$ states is higher by about 3000 cm^{-1} than that of CB and *o*-CT, the χ_f corresponds to the $v = 4$ level of the $^3\pi\pi^*$ state. The Franck–Condon overlaps, $\langle\chi_i|\chi_f\rangle^2$, are determined to be 0.21 and 0.16 for *m*-CT and *p*-CT, and for CB and *o*-CT, respectively.

The values of $\phi_{ISC}^{\pi\sigma^*}$ are also plotted against the charge on the Cl atom in Fig. 4; these are found to be smaller than those of $\phi_{ISC}^{\pi\pi^*}$ and are independent of the samples. This is also interpreted in terms of the Franck–Condon overlap between the S_1 and $^3\pi\sigma^*$ states. The situation of the potential surface crossing between these states is drawn in Fig. 5(c). The potential surfaces of the $^3\pi\sigma^*$ state are considered to be similar for all samples because the phosphorescence spectra from the $^3\pi\sigma^*$ states resemble each other. Obviously, the Franck–Condon overlaps between the S_1 and $^3\pi\sigma^*$ states are smaller than that of between the S_1 and $^3\pi\pi^*$ states. The values of $\phi_{ISC}^{\pi\pi^*}$ depend on the samples, which are correlated with the charge density on the Cl atom in the S_1 state and vibrational Franck–Condon overlap between S_1 and $^3\pi\pi^*$. However, the values of $^3\pi\sigma^*$ are independent of the samples, where the Franck–Condon overlaps are almost the same.

References

1 T. Ichimura, M. Iwai, and Y. Mori, *J. Phys. Chem.*, **92**, 4047 (1988).

2 T. Ichimura, Y. Mori, H. Sinohara, and N. Nishi, *J. Chem. Phys.*, **107**, 835 (1997).

3 J. T. Pinhey and R. D. G. Rigby, *Tetrahedron Lett.*, **16**, 1267 (1969).

4 M. A. Fox, W. C. Nicholas, and D. M. Lemal, *J. Am. Chem. Soc.*, **95**, 8164 (1973).

5 D. R. Arnold and D. C. Wong, *J. Am. Chem. Soc.*, **99**, 3361 (1977).

6 N. J. Bunce, P. J. Hayes, and M. E. Lemke, *Can. J. Chem.*,

61, 1103 (1983).

7 A. Brasinski and E. Latowska, *Rocz. Chem.*, **40**, 1747 (1966).

8 T. Ichimura and Y. Mori, *J. Chem. Phys.*, **58**, 288 (1973).

9 N. J. Bunce, P. J. Bergsma, M. D. Bergsma, W. DeGraaf, Y. Kumar, and L. Ravanal, *Org. Chem.*, **45**, 3708 (1980).

10 T. Takemura, Y. Yamada, M. Sugawara, and H. Baba, *J. Phys. Chem.*, **90**, 2324 (1986).

11 T. Ichimura, T. Hikida, and Y. Mori, *J. Phys. Chem.*, **79**, 291 (1975).

12 T. Takemura, Y. Yamada, and H. Baba, *Chem. Phys.*, **69**, 171 (1982).

13 E. C. Lim and S. K. Chakrabarti, *Mol. Phys.*, **13**, 293 (1967).

14 G. Castro and R. M. Hochstrasser, *J. Chem. Phys.*, **45**, 435 (1966).

15 D. S. McClure, *J. Chem. Phys.*, **17**, 905 (1948).

16 S. Niizuma, L. Kwan, and N. Hirota, *Mol. Phys.*, **35**, 1029 (1978).

17 H. Shinohara and N. Hirota, *J. Chem. Phys.*, **72**, 4445 (1980).

18 S. Nagaoka, T. Takemura, H. Baba, N. Koga, and K. Morokuma, *J. Phys. Chem.*, **90**, 759 (1986).

19 T. Okutsu, N. Kounose, H. Nakatsuka, T. Suzuki, T. Ichimura, and H. Hiratsuka, *J. Photochem. Photobiol. A: Chem.*, **115**, 243 (1998).

20 T. Okutsu, T. Kageyama, N. Kounose, J. Tsuchiya, and H. Hiratsuka, *Chem. Phys, Lett.*, **299**, 597 (1999).

21 S. L. Murov, I. Carmichael, and G. L. Hug,"Handbook of Photochemistry," 2nd ed, Maecel Dekker, New York (1993).

22 T. Takemura, M. Aikawa, H. Baba, and Y. Sindo, *J. Am. Chem. Soc.*, **98**, 2205 (1976).

23 J. B. Birks, "Photophysics of Aromatic Molecules," Wiley-Interscience, New York (1970), p. 304.

24 N. J. Turro, "Modern Molecular Photochemistry," The Benjamin/Cummings Publishing Co., California (1978).